EUROPEAN **S**YNCHROTRON **R**ADIATION **F**ACILITY

INSTALLATION EUROPEENNE DE RAYONNEMENT SYNCHROTRON

ESRF

Experiment Report Form

The double page inside this form is to be filled in by all users or groups of users who have had access to beam time for measurements at the ESRF.

Once completed, the report should be submitted electronically to the User Office using the **Electronic Report Submission Application:**

http://193.49.43.2:8080/smis/servlet/UserUtils?start

Reports supporting requests for additional beam time

Reports can now be submitted independently of new proposals – it is necessary simply to indicate the number of the report(s) supporting a new proposal on the proposal form.

The Review Committees reserve the right to reject new proposals from groups who have not reported on the use of beam time allocated previously.

Reports on experiments relating to long term projects

Proposers awarded beam time for a long term project are required to submit an interim report at the end of each year, irrespective of the number of shifts of beam time they have used.

Published papers

All users must give proper credit to ESRF staff members and proper mention to ESRF facilities which were essential for the results described in any ensuing publication. Further, they are obliged to send to the Joint ESRF/ ILL library the complete reference and the abstract of all papers appearing in print, and resulting from the use of the ESRF.

Should you wish to make more general comments on the experiment, please note them on the User Evaluation Form, and send both the Report and the Evaluation Form to the User Office.

Deadlines for submission of Experimental Reports

- 1st March for experiments carried out up until June of the previous year;
- 1st September for experiments carried out up until January of the same year.

Instructions for preparing your Report

- fill in a separate form for each project or series of measurements.
- type your report, in English.
- include the reference number of the proposal to which the report refers.
- make sure that the text, tables and figures fit into the space available.
- if your work is published or is in press, you may prefer to paste in the abstract, and add full reference details. If the abstract is in a language other than English, please include an English translation.

ESRF	**Experiment title:** Establishment and first tests of a new method for computed tomography with the use of analyser crystals	**Experiment number**: MI-882
Beamline: ID17	**Date of experiment**: from: 10-MAY-2007 at 8:00 to: 14-MAY-2007 at 8:00	**Date of report**:
Shifts: 12	**Local contact(s)**: Alberto Bravin	*Received at ESRF:*

Names and affiliations of applicants (* indicates experimentalists):

Timur Gureyev, CSIRO Manufacturing and Infrastructure Technology, Australia

*__Alberto Bravin,__ ESRF, France

*__Paola Coan__, ESRF, France

Yakov Nesterets, CSIRO Manufacturing and Infrastructure Technology, Australia

*__Konstantin Pavlov,__ School of Physics, Monash University, Australia

Andrew Stevenson, CSIRO Manufacturing and Infrastructure Technology, Australia

Stephen Wilkins, CSIRO Manufacturing and Infrastructure Technology, Australia

Report:

Experimental setup

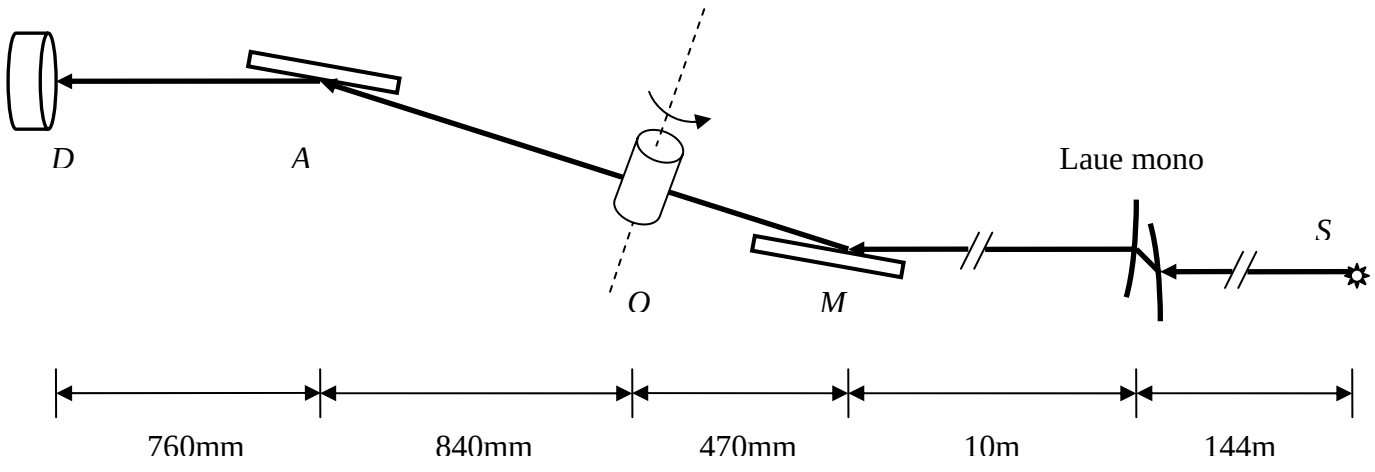

Fig.1 Experimental setup used for combined analyser-based/propagation-based computed tomography of small biological object (an insect) and of a test phantom (nylon fibres). X-ray energy used E = 25keV; symmetric Si(111) reflection in the monochromator (M) and analyser (A) crystals, θ_B = 4.53597°; detector effective pixel size 8.17μm.

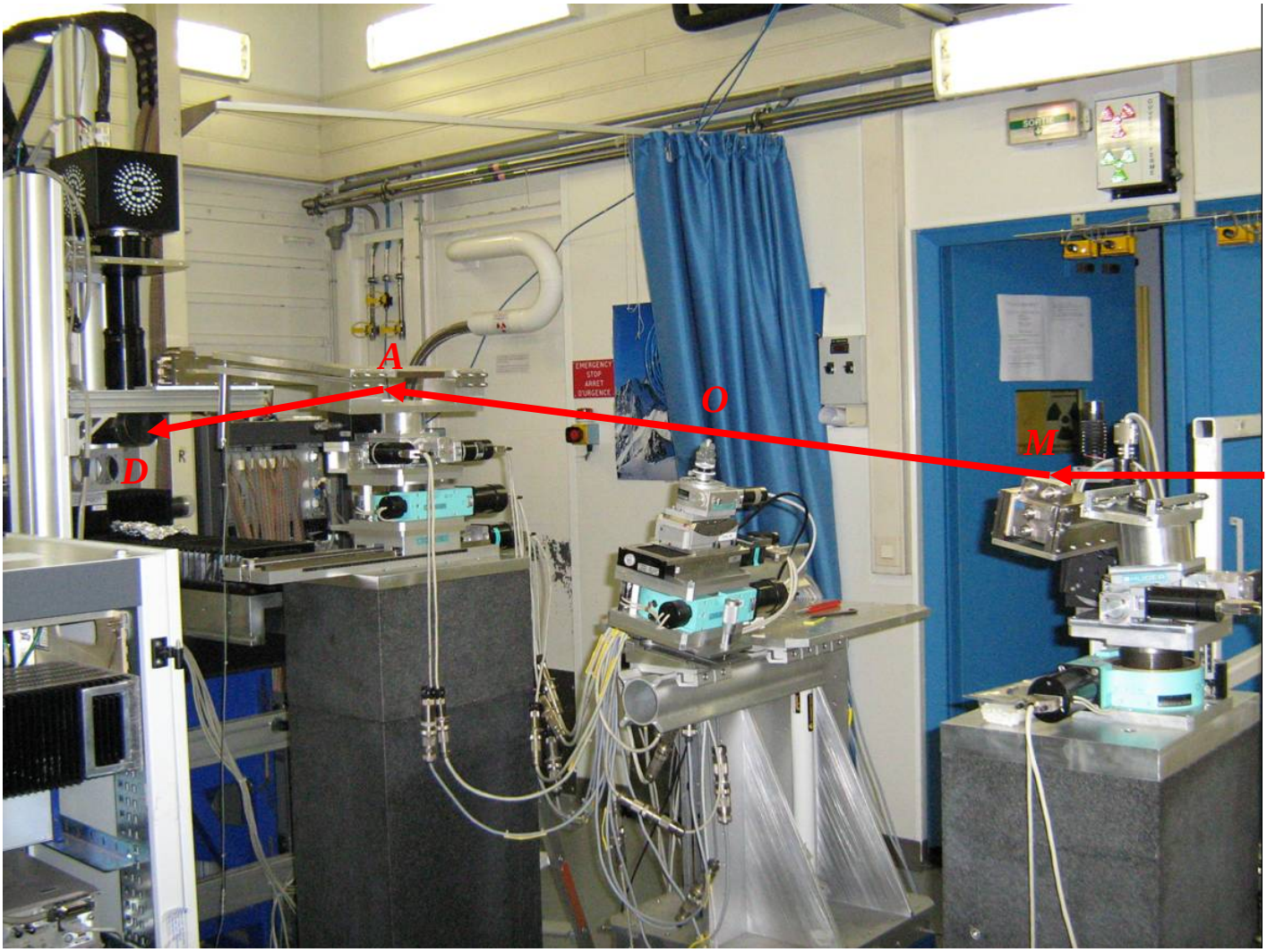

Fig.2 Photograph of the experimental setup. *M* – single-crystal monochromator, *O* – object stage with optional vertical (horizontal) rotation axis, *A* – single-crystal analyser, *D* – detector.

Monochromator: fixed-exit double-crystal bent-Laue Si(111) pre-monochromator, 144 m downstream from the source, and a plane Si(111) monochromator, 10 m downstream from the pre-monochromator. This combination of the bent-Laue monochromator and the single plane monochromator produced a very narrow beam with the vertical size about 1 mm in the object plane. This did not allow the whole object (phantom) to be irradiated (the outer diameter of the phantom was 2 mm) and only the central part of the phantom was used for CT.

Object: as the first test object, a small insect (unknown bug species) was used. The second test object was a well characterised phantom consisting of a hollow Perspex cylinder with the inner and outer radii equal to correspondingly 1800 and 2000 microns with four Nylon fibres inside (aligned along the cylinder). The diameters of the fibres are 100, 240, 330 and 420 microns. The schematic cross-section of the phantom is presented in Fig.5.

Analyser: plane silicon crystal, symmetric (111)-reflection.

Detector: a Frelon CCD-based camera with a chip containing 2048×2048 pixels. The camera is coupled with a “10 micron pixel optics” that has a 10 micron thick Gadox powder scintillation screen and the resulting effective pixel size is nominally of 7.5 micron in the image (with a spatial resolution of about 16 micron). In the experiment the effective pixel size was measured to be 8.17 microns. The dynamic range of the CCD camera was 14 bits.

Description of the experiment

The conducted experiment was aimed at the establishment and first tests of a new method for Computer Tomography (CT) with the use of analyser crystal (analyser-based imaging, ABI). The method differs from the already well established ABI-CT techniques **[1,2]** in that it: (a) uses a different experimental

geometry in which the axes of rotation of the sample and that of the analyser crystal are parallel to each other (as in **[3-5]**), (b) uses a new method for computer reconstruction of the 3-dimensional (3D) distribution of the complex refractive index inside the sample. The new reconstruction ABI-CT algorithm was recently presented by us at the SPIE conference **[6]**; it has been shown to be more numerically efficient and less sensitive to noise in the experimental data compared to previously known algorithms **[1-5]**. We were also intented to utilize a powerful new technique **[7]** for explicit accounting for the inevitable deviations of the incident X-ray beam from the idealized plane or spherical wave. We used one specially manufactured sample consisting of several different weakly absorbing components, namely a Perspex cylinder with Nylon fibres of 100, 240, 330 and 420 μm diameter, for the initial test of the method. This well-characterised sample was intended to use for initial tests and calibration of the new ABI-CT method.

High coherence and high intensity of the X-ray beam available at ID17 beamline have been utilised in order to enable the proposed ABI-CT experiment. Multiple (9 for the vertical rotation axis of the object and 15 for the horizontal one) 2D images have been collected at each angular position of the sample by rotating the analyser crystal through the rocking curve. This was arranged for compensation of the optical aberrations of the incident beam and reconstruction of the phase derivative in the object wave for each axial projection. The sample was rotated over 180 degrees with the angular step of 0.25 degree. For this experiment 25 keV energy and the Si(111) reflection of the analyser crystal were used. Data have been acquired with a CCD Frelon camera (8.17 micron effective pixel size and about 16 micron spatial resolution). Flat field images (with the sample removed) have been collected every 40 angular positions in order to account for possible changes in the beam intensity distribution over the duration of the experiment. For testing of the ABI-CT method, the object-to-detector distance ideally have to be minimized in order to minimize the propagation-based phase contrast. In the current experiment, the total object-to-detector distance was about 1.6 metres which did not allow complete suppression of the propagation-based contrast. Therefore the combined analyser-based/propagation-based version of the method **[7]** was planned to be used.

It was planned that the background- and dark-current-corrected images corresponding to all angular deviations of the analyser crystal would be acquired and processed according to the improved version **[7]** of the phase/amplitude retrieval algorithm in order to reconstruct the amplitude and phase derivative distribution in the object plane at each angular orientation of the samples. The following factors did not allow direct application of the multi-image phase/amplitude reconstruction method described in Ref. **[7]**:

1. Rotation axis of the analyser crystal did not lie on the crystal surface. This resulted in that different parts of the crystal surface have been irradiated at different angular deviations of the analyser crystal;
2. Detector position was fixed and the images were collected using different pixel windows (rows of pixels) in the CCD camera. Positions of the windows did not match the shift of the image due to analyser crystal rotation.

As a result, the images collected at each fixed axial position of the object but different angular positions of the analyser crystal were misaligned and had different flat-fields. As no special alignment markers were used in the object, all our attempts to align the images using correlation techniques have been unsuccessful. Therefore we could not use the multi-image phase/amplitude reconstruction technique. Instead, a less accurate phase reconstruction method for combined analyser-based/propagation-based imaging **[6,8]** for a homogeneous object was applied.

The retrieved amplitude and phase distributions have been used to determine the 3D distribution of the refractive index in the sample. These experimentally determined values of the refractive index have been compared with the theoretical estimations in order to verify the accuracy of the technique (see Results).

Results

As intended, the primary goal of this experiment was verification of the new experimental technique for quantitative amplitude/phase microscopy and tomography of non-crystalline samples using coherent hard X-rays and analyser crystal. The technique potentially allows non-destructive measurement of 3D distributions of the complex refractive index inside biomedical samples from the series of images collected at different angular deviations of the analyser crystal for each angular orientation of the sample.

First, combined ABI/PBI tomographic data for the first object (the bug) were acquired with the rotation axis of the analyser crystal perpendicular to the rotation axis of the object (“standard” geometry). Example raw image of the bug and the corresponding flat field image are presented in Fig.3a and Fig.3b respectively. Both images are 521×231 pixels and according to Fig.3b the field of view (FOV) in vertical direction was limited to about 700 microns (FWHM). Therefore only a narrow vertical slice of the bug (128

pixels high) was used for the reconstruction, see the normalised image in Fig.3c which was trimmed down to 512×128 pixels. Although several tomographic series, corresponding to 9 different angular positions of the analyser crystal, were acquired during the experiment, only the series corresponding to the position of the analyser at the top of its rocking curve was used for the tomographic reconstruction. Figure 3d shows a reconstructed contact image of the object corresponding to Fig.3c, taking into account only the effect of free-space propagation and neglecting the effect of the analyser crystal. The latter was possible as the images were acquired at the top of the analyser rocking curve. Two sinograms corresponding to the central slice (in Fig.3c) of the object, using correspondingly the original images (like one shown in Fig.3c) and the reconstructed contact images (similar to that shown in Fig.3d), are presented in Fig.3e and Fig.3f respectively. Standard filtered backprojection (FBP) algorithm was then applied to these sinograms and the results are presented in Fig.3g and Fig.3h respectively. The corresponding 3D representations of the reconstructions of the whole set of data are shown in Fig.4a and Fig.4b (correspondingly without and with the contact images reconstruction).

In the second configuration the rotation axis of the analyser-crystal was parallel to the rotation axis of the object ("new" geometry). Fourteen tomographic data sets (for 14 different deviations of the analyser-crystal) for both test objects were collected. We consider the results for the phantom presented in Fig.5 corresponding to the angular position of the analyser-crystal at the negative slope (at half maximum) of its rocking curve. An example sinogram calculated using the original images of the phantom is shown in Fig.6a and the corresponding result of applying the FBP algorithm to this sinogram is shown in Fig.6c. Also, we have reconstructed the contact images of the object using the algorithm proposed in Refs.**[6,8]**. An example sinogram, for the same slice as in Fig.6a, using the reconstructed contact images is shown in Fig.6b and the corresponding FBP reconstruction of this slice is presented in Fig.6d. Rotation axis of the object is indicated by the red cross in Fig.6c and Fig.6d. It was found to be located 241 microns from the centre of the FOV (this distance is indicated by the blue line). White dashed circle in Fig.3c and Fig.3d indicates the part of the object which was within the FOV in all projections (we call this circle a region of interest (ROI) and in this experimental data set the diameter of this ROI was limited to 564 microns). As the ROI is located inside the object, the data shown in Fig.6 present an example of quasi-local tomographic reconstruction **[9]** where the tomographic reconstruction error depends on the distance of the point of interest from the boundary of the ROI. Analysis of data presented in Fig.6d gave the following value for the imaginary part β of the refractive index of the smallest fibre, $\beta = (1.43 \pm 0.09)\times10^{-10}$ while the theoretical value for the 25keV energy used in our experiment $\beta_{theor} = 1.41\times10^{-10}$. Thus a good quantitative reconstruction for the phantom has been achieved using this data set.

References

1. F.A. Dilmanian, Z. Zhong, B. Ren, X.Y. Wu, L.D. Chapman, I. Orion and W.C. Thomlinson, Phys. Med. Biol. **45**, 933 (2000).
2. K.M. Pavlov, C.M. Kewish, J.R. Davis and M.J.Morgan, J. Phys. D: Appl. Phys. **34**, A168-A172 (2001).
3. I. Koyama, A. Momose, J. Wu, T.T. Lwin and T. Takeda, Japan J. Appl. Phys. **44**, 8219-8221 (2005).
4. P.P. Zhu, J.Y. Wang, Q.X. Yuan, W.X. Huang, H. Shu, B. Gao, T.D. Hu and Z.W. Wu, Appl. Phys. Lett. **87**, 264101 (2005).
5. Z.F. Huang, K.J. Kang, Z. Li, P.P. Zhu, Q.X. Yuan, W.X. Huang, J.Y. Wang, D. Zhang and A.M. Yu, Appl. Phys. Lett. **89**, 041124 (2006).
6. Timur E. Gureyev, Glenn R. Myers, Yakov I. Nesterets, David M. Paganin, Konstantin M. Pavlov, Stephen W. Wilkins, Developments in x-ray tomography V, 13–17 August 2006, San Diego, CA USA.
7. Ya.I. Nesterets, P. Coan, T.E. Gureyev, A. Bravin, P. Cloetens and S.W. Wilkins, Acta Cryst. A **62**, 296-308 (2006).
8. Ya.I. Nesterets, T.E. Gureyev and S.W. Wilkins, Appl. Phys. Let. **89**, 264103 (2006).
9. T.E. Gureyev, Ya.I. Nesterets, S.C.Mayo and S.W. Wilkins, Opt. Commun. **280**, 39-48 (2007).

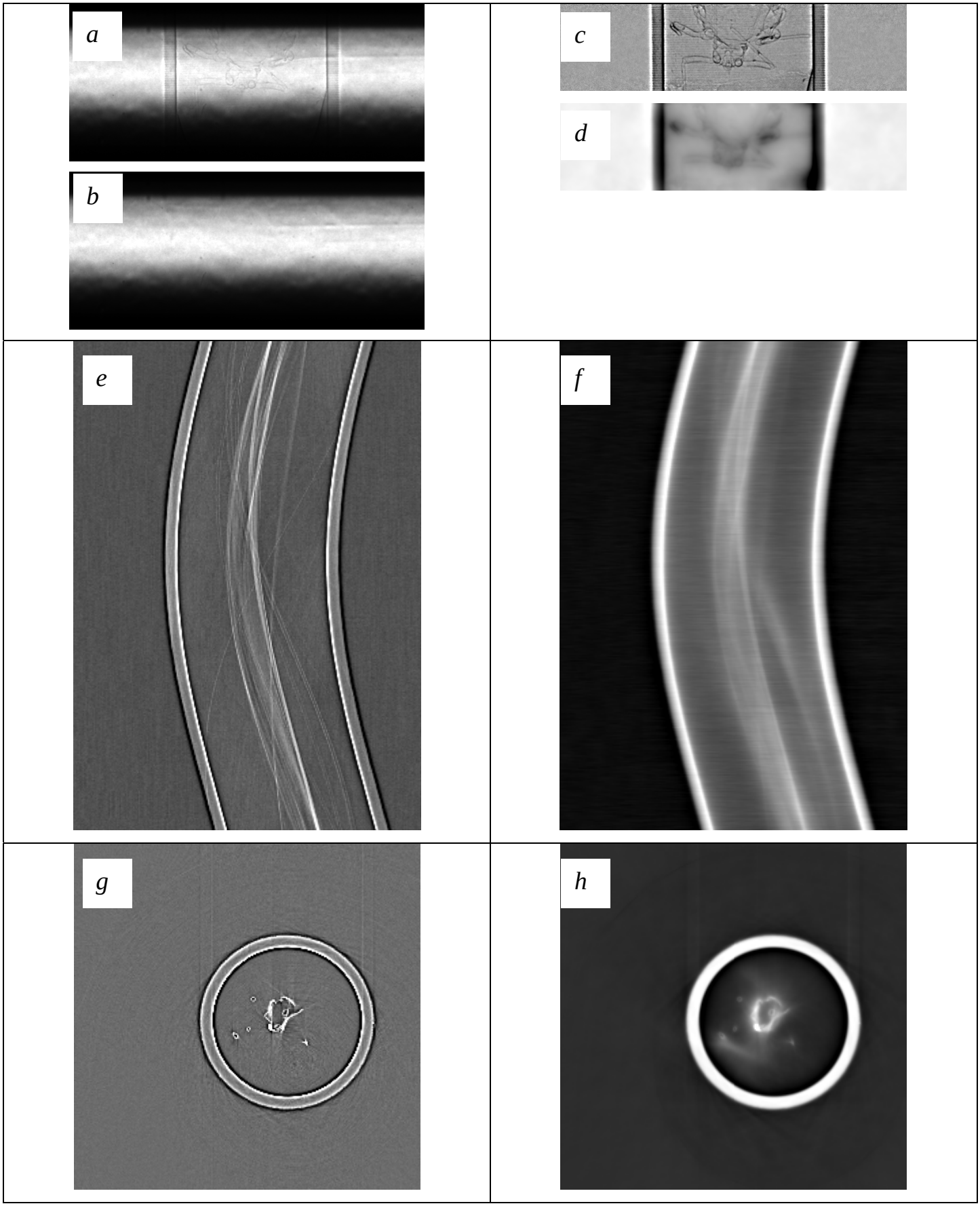

Fig. 3 Analyser-crystal set at top of the rocking curve, vertical rotation axis of the object. Representative raw image (a single projection of 721) of the bug (a), the corresponding flat field (b) and the normalised (and trimmed) image before (c) and after (d) amplitude reconstruction; sinograms (512 pixels × 721 projections) of the central slice using the images before (e) and after (f) amplitude reconstruction, and the corresponding FBP reconstructions (512×512 pixels) of the slice, (g) and (h) respectively.

a *b*

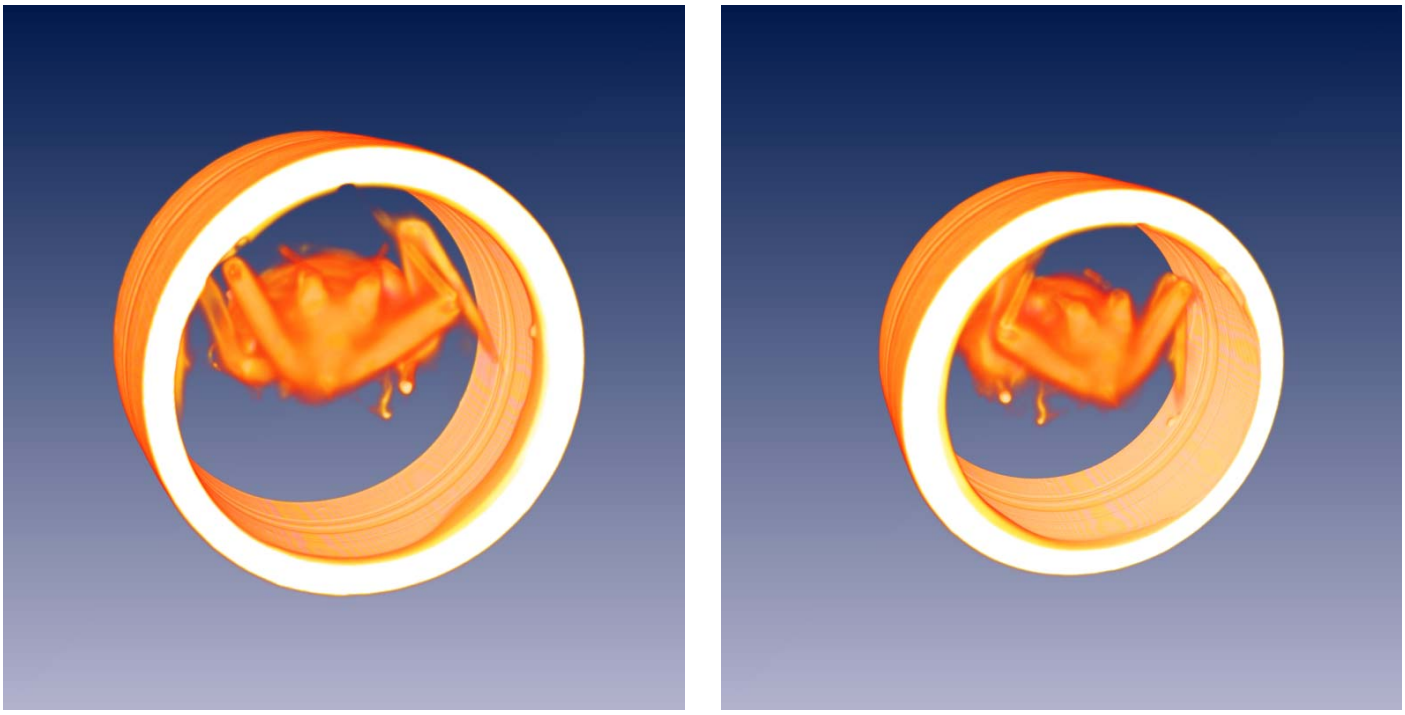

Fig.4 Three-dimensional rendering of the reconstruction (using FBP algorithm) applied to the original images (a), collected with the analyser-crystal positioned at the top of its rocking curve, and to the reconstructed contact images (b) using the TIE-based reconstruction algorithm **[6]**.

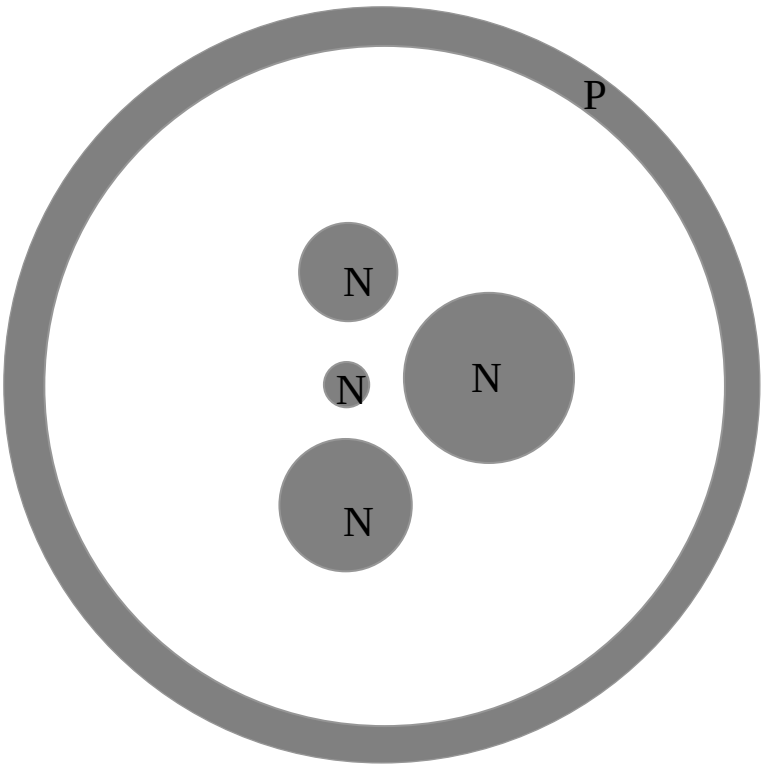

Fig.5 Schematic representation of the phantom used in our experiments. Diameters of the Nylon fibres (N): 100 μm, 240 μm, 330 μm and 420 μm. Outer and inner diameters of the Perspex hollow cylinder (P): 2000 μm and 1800 μm.

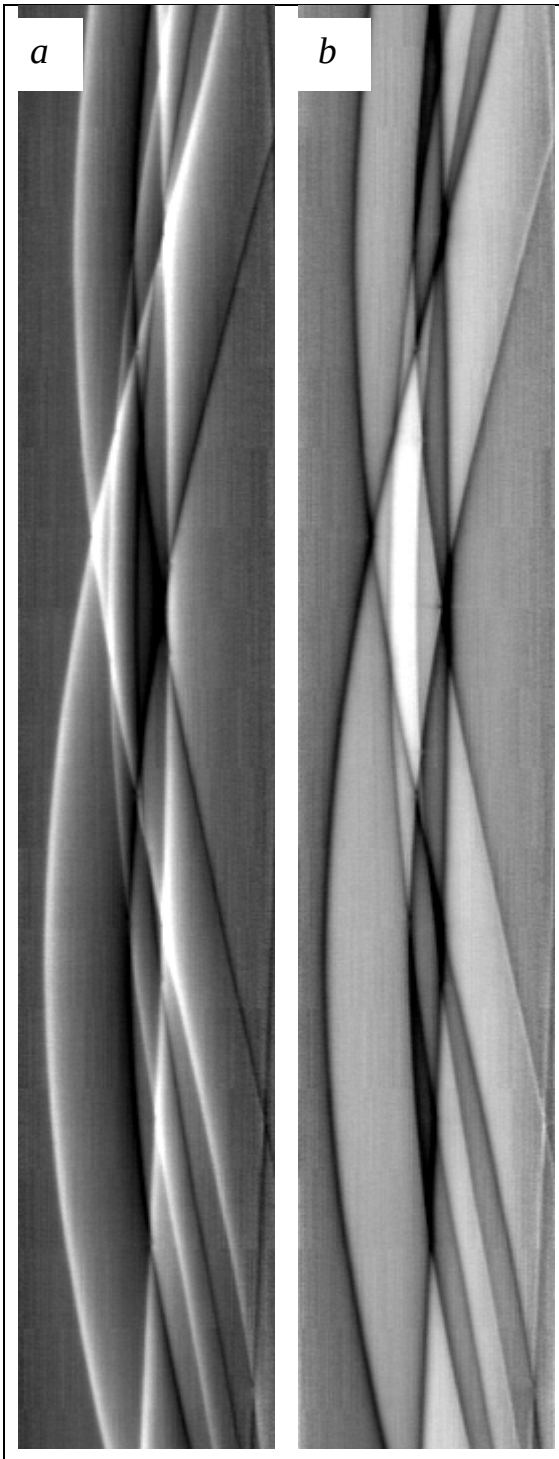

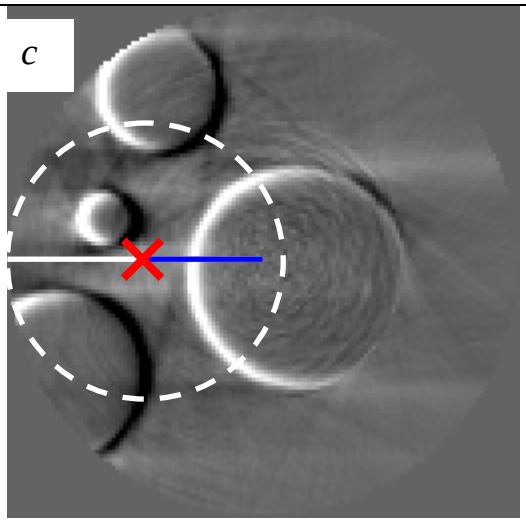

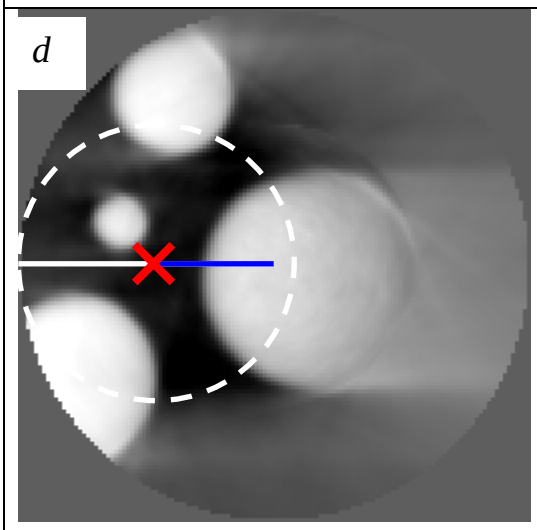

Fig. 6 Sinogram (128 pixels × 721 projections) of a representative single slice of the object, calculated using the original (unprocessed) images (a) and filtered (processed) images (b) and the corresponding FBP reconstructions (128×128 pixels) of the slice (c,d).